Available online at www.qu.edu.iq/journalcm
JOURNAL OF AL-QADISIYAH FOR COMPUTER SCIENCE AND MATHEMATICS
ISSN:2521-3504(online) ISSN:2074-0204(print)

Neutrosophic Domain for Image Zero Watermarking

Hussein Kadhim Abdali[a], Areej M. Abduldaim[a,*], Matheel E. Abdulmunim[b]

[a]*Department of Mathematics and Computer Applications, College of Applied Sciences, University of Technology, Al-sinaa Street, Baghdad 10001, Iraq.Email: as.24.35@grad.uotechnology.edu.iq and Areej.M.Abduldaim@uotechnology.edu.iq*

[b]*Multimedia and Digital Media Department, College of Computer Sciences, University of Technology, Al-sinaa Street, Baghdad 10001, Iraq.Email: matheel.e.abdulmunim@uotechnology.edu.iq*

ARTICLE INFO

Article history:
Received: 02 /06/2026
Rrevised form: 17 /06/2026
Accepted : 18 /06/2026
Available online: 30 /06/2026

Keywords:

Membership Functions,

Neutrosophic Domain,

Image Zero Watermarking,

Zero Watermark Construction,

Watermark Recovery.

ABSTRACT

In our time, the use of various technological application systems has become an accepted and indispensable necessity. Naturally, the use of images in these applications is a priority due to the significant impact of image circulation, whether for medical, industrial, economic, or, of course, social and personal purposes. Therefore, the ease with which this vast amount of data is shared has led to significant challenges in terms of security, intellectual property rights protection, and other areas. Consequently, watermarking technologies, especially zero-based watermarking, have become an ideal solution for preserving images, provided that ownership is securely verified without any alteration to the original images. This research aims to propose a developed zero-watermarking model using: 1- A neutrosophic domain, which is used to extract important image features and use them to generate new features. 2- Calculating the average of each block to create a new, more stable feature matrix. Initially, the image is converted to a neutrosophic domain, and the component T is selected and divided into non-overlapping blocks, each of size 4x4. Accordingly, a feature matrix is created whose elements are the average values of each block and converted to binary form, where the watermark is merged with it through XOR to build the zero watermark.

MSC..

https://doi.org/ 10.29304/jqcsm.2026.18.22948

1. Introduction

The increasing importance of protecting and securing images and intellectual property rights has arisen from the widespread use of digital images in various fields of life, including communications, multimedia platforms, and military and medical applications. This massive expansion has caused serious concerns due to the ease with which images can be illegally shared, copied, and modified [1,2]. Hiding information in the form of a logo in traditional watermarking technology corrupts the image, making it fragile and vulnerable to damage if exposed to any attack [3]. Therefore, to overcome these gaps and to preserve the original image without any damage, methods for zero watermark technology were improved and developed to guarantee copyright and ownership rights [4]. This leads to these technologies being among the most active research fields due to their security features in terms of image verification and their importance in security [5].

The use of the neutrosophic domain in image processing has recently become noteworthy due to its effective ability to manipulate images through three components, namely: the truth, indeterminacy, and falsity. Unlike the use of conventional transformations such as Discrete Wavelet Transform (DWT) and Discrete Cosine Transform (DCT), which depend on the nature of the pixel, the neutrosophic domain specifically differentiates between noise-sensitive

∗Corresponding author: Areej M. Abduldaim
Email addresses: Areej.M.Abduldaim@uotechnology.edu.iq
Communicated by 'sub etitor'

areas and important image structures [6,7]. Image segmentation applications can be improved by using the neutrosophic domain to partition the image regions. This approach guarantees that the modeling is effective via the truth, indeterminacy, and falsity components [8]. Therefore, the process used gives us accuracy in segmentation while simultaneously preserving the structural boundaries used, leading to highly reliable identification of object regions [9]. Based on all of the above, neutrosophic theory can be considered an effective mathematical approach for developing many systems, such as clustering [10], edge detection [11], and a content-based retrieval system [12].

The main part of the proposed contribution lies in employing the neutrosophic domain and using it as a mathematical transformation to extract image features by splitting the image into blocks through a unified approach to zero watermarking to securely protect image copyrights. This gives us the ability and flexibility at the same time to obtain the features needed for the zero-watermark construction, depending on the purpose for which it is designed, whether it be to protect property or copyright, or to detect forgery and manipulation of images. In the proposed technique, the truth component image utilizes the neutrosophic domain, which is obtained to extract more stable and discriminative features to be less sensitive to common image distortions. Moreover, the computation of the average for each nonoverlapping block enhances the feature uniformity and the Computational Performance Evaluation. As a result, the proposed technique achieves an effective balance between robustness, security, and image preservation without modifying the original cover image.

2. Related Work

The digital watermarking techniques are generally divided into spatial-domain and transform-domain approaches. Spatial-domain methods directly modify image pixels and provide simple implementation with low computational complexity, while transform-domain methods such as DWT, DCT, and SVD offer higher robustness and imperceptibility against image processing attacks [13,14]. These techniques are widely used for copyright protection, authentication, and multimedia security applications [15,16]. To the best of our knowledge, there is limited research on the application of the neutrosophic concept in the field of watermarking in general [17, 18]. In that paper, the neutrosophic concept is used to evaluate the similarity between the input and recovered watermark.

Previous literature has not clearly addressed the use of the neutrosophic concept as a tool for image transformation into a new domain for image watermarking techniques, while most of what has been published has been about its use as an image transformation for the image segmentation process [18-20].

Extracting robust image features instead of embedding watermark information into the cover image in the zero-watermarking methods preserves the original image unmanipulated. Algebraic feature extraction, transform-based, and statistical methods are used in the common techniques to construct the zero watermark [21-23]. As the needed application of the watermarking paradigm, robust zero-watermarking systems are designed for copyright protection and authentication, fragile systems, and semi-fragile systems for tampering detection [24, 25].

3. Background

3.1 Neutrosophic Theory

Florentin Smarandache introduced the Neutrosophic Theory to represent an advanced mathematical concept that concerns truth (T), indeterminacy (I), and falsity (F). The theory is based on the concept that each situation or element can possess independent degrees of truth (T), falsity (F), and indeterminacy or uncertainty (I), providing greater flexibility compared to classical or traditional fuzzy logic [6].

This structure provides broad capabilities for analyzing complex problems, and Neutrosophic Sets have been applied in various fields, including multi-criteria decision making, artificial intelligence, uncertain data processing, and decision support systems [26-28].

3.2 Neutrosophic Domain

In digital image processing, each pixel can be represented in the Neutrosophic Domain using three membership values: truth (T), indeterminacy (I), and falsity (F). When an image is transformed into this domain, a pixel $P(i,j)$ in the neutrosophic image is represented as follows [7]:

$$P_{NS}(i,j) = \{T(i,j), I(i,j), F(i,j)\}.$$

The three membership values are defined by the following equations [7]:

Truth membership (T): $T(i,j) = \frac{\bar{g}(i,j) - \bar{g}_{min}}{\bar{g}_{\max} - \bar{g}_{\min}}$,

where $g(i,j)$ is the local mean intensity of the pixel within a $w \times w$ window around (i, j):

$$\bar{g}(i,j) = \frac{1}{w \times w} \sum_{m=i-w/2}^{i=w/2} \sum_{n=j-w/2}^{j+w/2} g(m,n)$$

These parameters, $\bar{g}_{\max}$ and $\bar{g}_{min}$ represent the limits of maximum illumination intensity within the image components. Specifically, $\bar{g}_{\max}$ indicates the highest illumination value, while $\bar{g}_{min}$ indicates the lowest illumination value. These parameters are dynamically adjusted to reflect the actual minimum and maximum pixel intensity in the input image.

Indeterminacy membership (I):

$$I(i,j) = \frac{\delta(i,j) - \delta_{\min}}{\delta_{\max} - \delta_{\min}}, \delta(i,j) = abs(g(i,j) - \bar{g}(i,j))$$

Falsity membership (F):

$$F(i,j) = 1 - T(i,j)$$

This representation allows each pixel to be processed in the neutrosophic domain while accounting for indeterminacy, forming the basis for image segmentation using neutrosophic logic [7].

After converting a standard digital image to a neutrosophic domain, we obtain three separate matrices: the truth matrix (T), the indeterminacy matrix (I), and the falsity matrix (F). These three matrices contain the values for each pixel. To provide a localized structural perspective on this digital data, a representative subset extracted from these underlying matrices is listed in the following tables.

3.3 Normalized Correlation (NC)

Normalized correlation is a metric that measures the similarity between two images W and W'.

$$NC = \frac{\sum_{m=1} \sum_{n=1} W \times W'}{\sqrt{\sum_{m=1} \sum_{n=1} W^2} \times \sqrt{\sum_{m=1} \sum_{n=1} W'^2}}$$

where W is the elements of the original watermark and W' is the elements of the extracted watermark.

3.4 The Logistic Map

The Logistic Map is a nonlinear mathematical model used to study dynamic behavior and chaotic systems. It is based on iterating an initial value to generate a time series.

$$x_{n+1} = r x_n (1 - x_n)$$

where r is the control parameter that determines the system behavior (stability, oscillation, or chaos), and x_1 is the initial value of the system, usually chosen in the range $0 < x_1 < 1$, from which the iteration process begins. In this work $r = 3.7, x1 = 0.3,$ and the parameter n represents the length of the chaotic sequence

3.5 The Attacks Used in this Research

In this research, we used three categories of attacks:

a- Noise attacks:

i. Salt and pepper noise (density was 0.01): Salt and pepper noise are an example of statistical noise, although it contaminates the image with a very different Probability Density Function (PDF). However, it presents itself as randomly occurring white and black pixels in an image

ii. Gaussian noise (the variance was 0.00017): The Gaussian noise attack is a statistical noise that adds a noise signal to an image with different variances to intentionally corrupt the image

iii. Poisson's noise: Poisson noise or shot noise is a type of electronic noise. It occurs when the number of electrons in an electronic circuit or photons in an optical device is small enough to give rise to detectable statistical fluctuations in measurement.

$$f(k,\lambda) = \frac{\lambda^k e^{-\lambda}}{k!}$$

iv. Speckle Noise (variance 0.001): Speckle is a multiplicative noise attack that inherently exists in and degrades the quality of the image, distributed random noise with mean 0 and a different number of variances.

b- Filter attacks:

i- Gaussian low-pass filter with a 2 × 2 kernel and σ = 0.5 was applied: The Gaussian method of image blurring is popular and often implemented filter. Gaussian Blurring produces resulting images appearing to contain a more uniform level of smoothing.

$$G(x,y) = \frac{1}{2\pi\sigma^2}\, e^{-\frac{x^2+y^2}{2\sigma^2}}$$

ii- Motion filter (Linear motion of camera was Length = 20pixels, Angle of camera motion was theta = 45 degrees):A uniform motion filter can be simulated by convolving an image with a motion blur kernel, commonly known as the Point Spread Function (PSF), which is classified as a distortion-based filtering attack.

iii- Average filter (Size of the filter was [2 2]): The average filter is a filter that uses a mask over each pixel in the image. Each of the components of the pixels which fall under the mask is averaged together to form a single pixel. This new pixel is then used to replace the pixel in the image studied. The Mean Filter is poor at maintaining edges within the image.

$$f\hat{}(x,y) = (1/MN)\, \Sigma_{(s,t)\in Sxy}\, g(s,t)$$

iv- Median filter (the size was [2 2]): Median Filtering is an image processing technique which aims at reducing the presence of noise in an image, hence enhancing the image quality. The median filter is the best-known order-statistic filter

c- Image-Processing Attacks

i- JPEG compression with a quality factor (QF) of 100: Image compression is used to compress and reduce the size or reduce the cost of bandwidth before still images are transmitted for storage and transmission. However, image compression can be considered as an unintentional attack.

ii- Histogram equalization: The histogram equalization attack is a method in image processing, in contrast. Mostly, it can be performed with the help of a histogram to specify the image type.

4. Proposed Neutrosophic Zero-Watermarking Mechanism

In this section, a new zero watermarking mechanism is proposed to construct a zero watermark and recover a watermark image using the neutrosophic domain given in [7].

4.1 Zero Watermark Construction

The zero watermark construction utilizing the neutrosophic domain is given below and demonstrated in Figure 4.

The Zero Watermark Construction Algorithm
Start **Step 1:** Input and convert the original image of size 256×256 into a grayscale image. **Step 2:** Input binary watermarks of size 64×64. **Step 3:** Convert the original image to the neutrosophic domain using the membership functions to obtain the matrix of the neutrosophic component $\boldsymbol{T}$. $$\boldsymbol{T(i,j)} = \frac{\bar{g}(i,j) - \bar{g}_{min}}{\bar{g}_{max} - \bar{g}_{min}}$$ **Step 4:** Select and divide the Neutrosophic component T into 64×64 blocks, each block is of size 4×4. **Step 5:** For each block, we calculate the average of all pixels within the block; the resulting value is the feature of that block. $$Average = \frac{1}{N} \sum_{i=1}^{N} \text{Pixel}_i$$ **Step 6:** We place the average values for each block into a new matrix, denoted as U, of size 64X64, such that each block represents the average of its pixel values. **Step 7:** Convert matrix $\boldsymbol{U}$ into a binary matrix $\boldsymbol{K}$ where $\boldsymbol{1 \leq i \leq n}$ and $\boldsymbol{1 \leq j \leq n}$. **Step 8:** Perform an XOR operation between K and the binary watermark W to get the secret share M. **Step 9:** For more security, the chaotic logistic map is used on $\boldsymbol{M}$ to change the values placed to get the secret share End

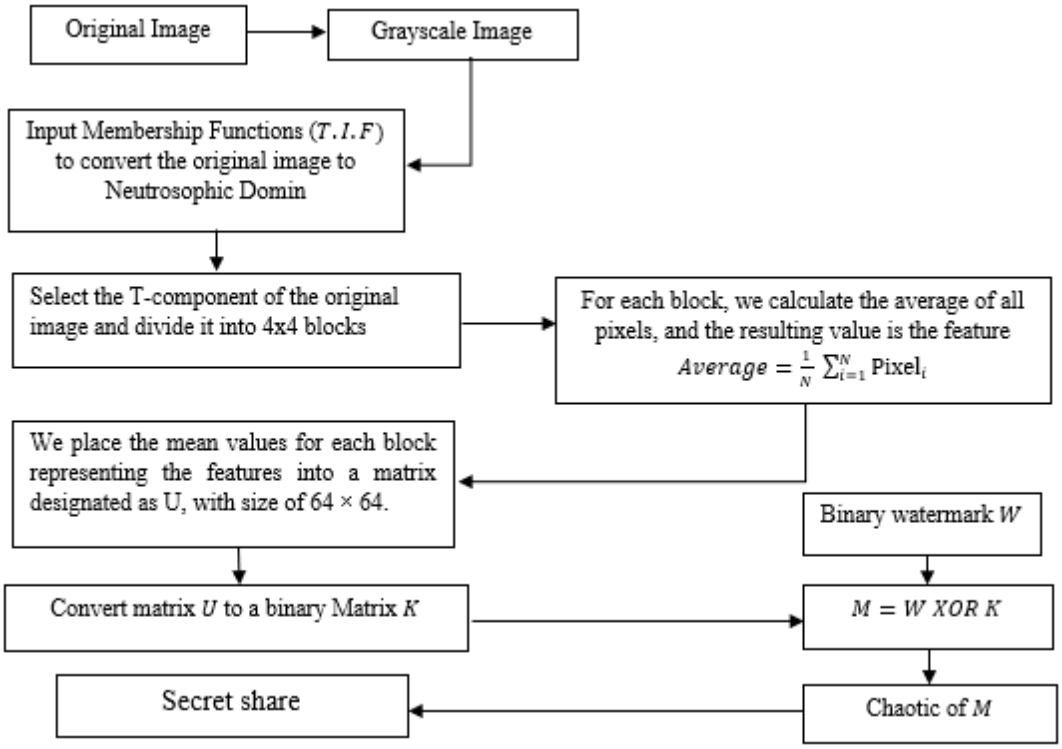

Figure 1: The diagram of the zero-watermark construction.

4.2 Watermark Recovery

The watermark recovery utilizing the neutrosophic domain is given below and demonstrated in Figure 5.

The Watermark Recovery Algorithm
Start **Step 1:** Enter the suspected image of size 256×256, transform it into a gray-level form. **Step 2:** Input the secret share and apply the chaotic logistic map on the secret share to get the Matrix M. **Step 3:** Convert the original image to the neutrosophic domain using the membership functions to obtain the matrix of the neutrosophic component $\boldsymbol{T}$. $$\boldsymbol{T}(\boldsymbol{i},\boldsymbol{j}) = \frac{\bar{g}(i,j) - \bar{g}_{min}}{\bar{g}_{max} - \bar{g}_{min}}$$ **Step 4:** Select and divide the Neutrosophic component $\boldsymbol{T}$ into 64×64 blocks, each block is of size 4×4. **Step 5:** For each block, we calculate the average of all pixels within the block; the resulting value is the feature of that block.

$$Average = \frac{1}{N} \sum_{i=1}^{N} \text{Pixel}_i$$

Step 6: We place the average values for each block into a new matrix, denoted as U, of size 64X64, such that each block represents the average of its pixel values.

Step 7: Convert matrix $\boldsymbol{U}$ into a binary matrix $\boldsymbol{K}$ where $\boldsymbol{1 \leq i \leq n}$ and $\boldsymbol{1 \leq j \leq n}$.

Step 8: Apply the XOR operation between the binary features $\boldsymbol{K}$ and the secret share$\boldsymbol{M}$ to extract the Watermark.

End

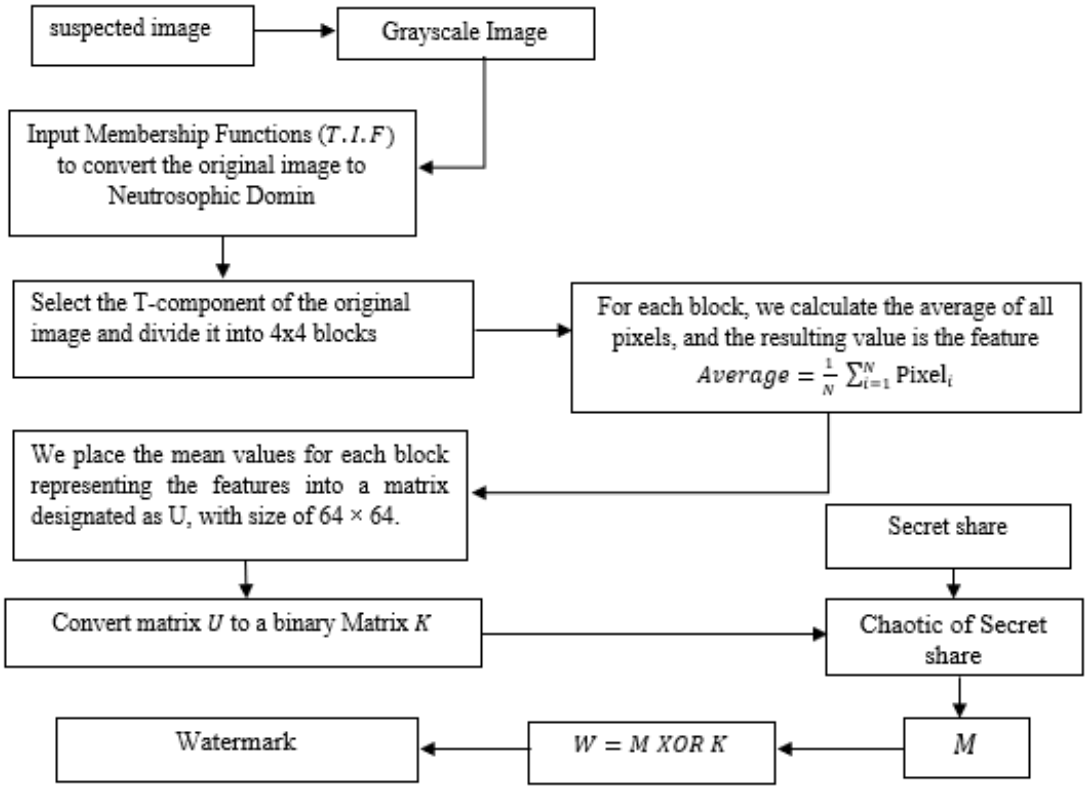

Figure 2: The diagram of the authentication procedure.

The proposed zero watermarking method consists of two steps: first, watermark generation and extraction. The input image is converted to grayscale and then to a neutral field using the proposed affiliation functions, where only the truth component (T) is selected. Image T is divided into non-overlapping $4x4$ blocks, and the average value of each block is calculated as a representative feature. These features are then sorted into a $64x64$ matrix U, which is then converted to a binary matrix to produce a feature matrix K. The binary watermark W is then combined with K using an XOR process to generate the zero watermark M, which is obfuscated using a chaotic map and stored as a secret quotient. In the verification process, the same feature extraction is performed on the suspect image to obtain K. The stored secret quotient is decoded to recover M, and the watermark is reconstructed using an XOR process between K and M. The system evaluates the similarity between extracted and original watermarks to determine the integrity, security, and authenticity of the image.

Using average-mass features provides a concise representation of the image structure, while the neutral $T-component$ enhances feature stability by highlighting important image details and suppressing non-important variations.

5. Security and Robustness Analysis and Complexity

5.1 Security Analysis

The proposed zero-watermarking framework provides a high level of security by avoiding direct embedding of watermark information into the host image. Instead, the watermark is combined with the extracted feature matrix through the XOR operation to generate an intermediate share M, which is further protected using chaotic scrambling. Since the secret share depends on both the watermark and the image features extracted from the neutrosophic domain, unauthorized users cannot reconstruct the watermark without access to the correct secret share and extraction procedure. In addition, the chaotic scrambling stage increases randomness and sensitivity to initial conditions, making the system resistant to forgery, statistical analysis, and unauthorized watermark estimation attacks. Consequently, the proposed framework improves confidentiality and secure ownership verification while preserving the original image completely.

5.2 Robustness Analysis

The robustness of the proposed method is achieved through the use of neutrosophic-domain representation and block-based statistical feature extraction. The truth component T emphasizes stable structural information while reducing the influence of noise-sensitive regions and uncertainty. Furthermore, the averaging operation performed on non-overlapping 4×4 blocks produces stable feature values that are less affected by common image processing operations such as filtering, compression, and noise attacks. Since the watermark is generated from global structural features rather than individual pixels, the proposed method maintains reliable watermark recovery even under moderate image distortions. The integration of chaotic scrambling additionally enhances the resistance against intentional manipulation and tampering attacks, improving the overall reliability of the authentication process.

5.3 Computational Complexity Analysis

The image size and the procedures implemented to extract the features and the zero watermark construction determine how to compute the complexity of the proposed zero-watermarking algorithm. For each non-overlapping 4×4 blocks in the grayscale image of size $N \times N$, the grayscale conversion and neutrosophic transformation stages process each pixel once; therefore, their computational complexity is $O(N^2)$. Similarly, the partitioning of the truth component T into blocks and the computation of the average value for each block require visiting all image pixels, resulting in a complexity of $O(N^2)$. The generated feature matrix U, a binary matrix K, XOR operation with the watermark W, and chaotic scrambling are applied to matrices of size $\frac{N}{4} \times \frac{N}{4}$ leading to complexities proportional to $O(N^2)$.

Consequently, the total computational complexity of the proposed framework is given by $O(N^2)$ which indicates that the algorithm has linear complexity with respect to the number of image pixels. This demonstrates that the proposed method is computationally efficient and suitable for practical image copyright protection and authentication applications. The space complexity is also $O(N^2)$, due to the storage requirements of the neutrosophic components and feature matrices.

6. Experimental Results and Discussion

This section presents the results obtained from the proposed method in the field of neutrosophic domain. The algorithm's performance was evaluated on numerous images. The method was also tested against various types of attacks.

Baboon	Peppers	Girl	VillageRoad

Figure 3: The images used in this work

A binary watermark image of size 64×64 was used in the experiments and converted into a binary sequence before generating the zero watermark. The watermark is a QR code generated for the link to the University of Technology website: https://uotechnology.edu.iq/en/

Figure 4:The QR Code of the Website

Table 1: The NC Values with no Attacks

Images	Baboon	Peppers	Girl	Village Road
NC	1	1	1	1

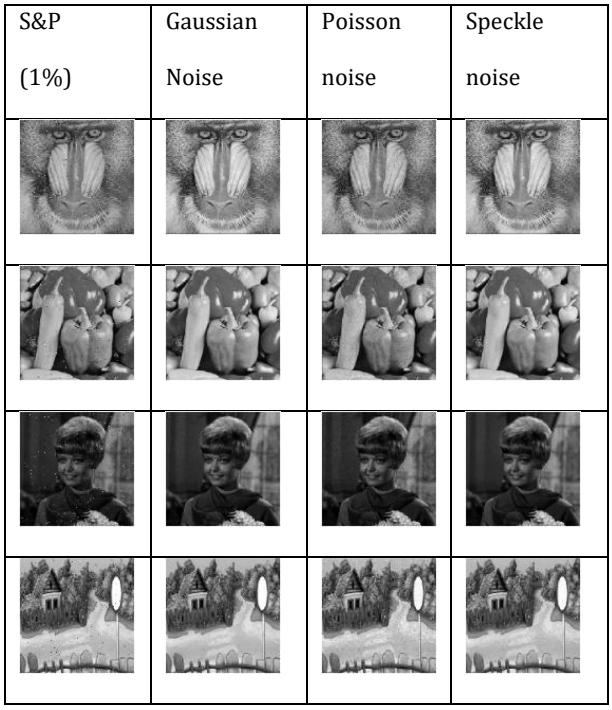

Figure 5: The images used after the noise attacks

Gauss LPF	Motion filter	Average filter	MED filter
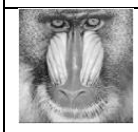		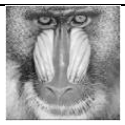	
			
			
			

Figure 6: The images used after the filter attacks

JPEG Compression Quality (100)	Histogram Equalization
	
	
	
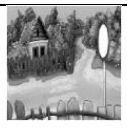	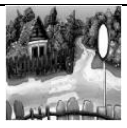

Figure 7: The images used after the image-processing attacks

6.1 The Results of Applying the Neutrosophic Domain on Images

In this section, the neutrosophic domain is applied to the images adopted in this work, and sub-images are presented of the three components: T, I, and F for the Baboon image.

This method is applied to the four images used in the project. The original RGB images, 256 x 256 pixels, were loaded into MATLAB and converted to grayscale to improve and simplify the computational processing. The structural membership functions truth (T), indeterminacy (I), and falsity (F) are calculated in a precise and systematic manner for each pixel, using the mathematical formulas mentioned. The result was a three-dimensional representation for each pixel (T, I, F) instead of a single representation. The result of this application is shown in Figure 1.

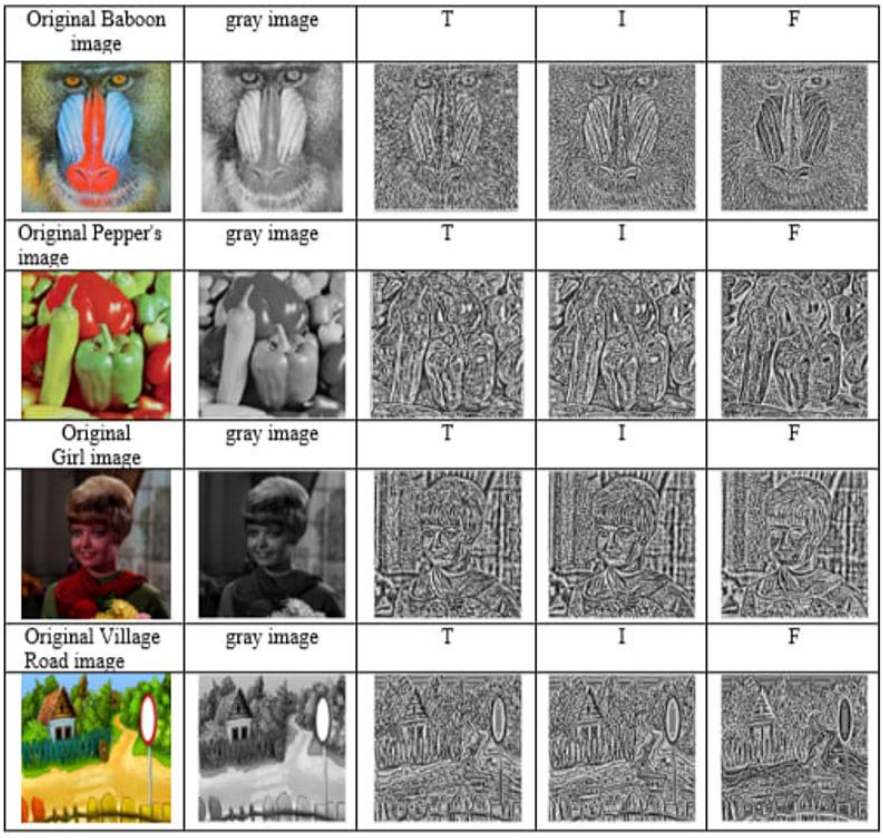

Figure 8: Application to represent the conversion of the original images to (T, I, F)

Table 2: Truth Membership Matrix (T) of the Baboon image

	1	2	3	4	5	6	7	8	9	10
1	0.9597	0.0084	0.9847	0.0013	0.0835	0.9918	0.9635	0.4770	1.0000	0.5564
2	0.9539	0.0420	0.1986	0.0023	0.8833	0.0443	9.6921e-05	1.0422e-04	0.9663	0.7595
3	0.9698	0.9922	0.0777	0.0049	0.4756	0.3542	0.6088	1.1975e-04	0.1122	0.4131
4	0.0159	1.0000	0.9813	0.0043	0.6933	0.7124	0.5090	0.2333	0.0642	0.4539
5	0.0069	0.9477	0.9974	0.0069	0.7868	0.9998	0.8625	0.9783	0.0421	0.8489
6	0.0118	0.0293	0.2780	0.1052	0.8942	0.9999	0.9998	0.8072	0.3195	0.4264
7	0.0060	0.9910	0.0776	0.3333	0.9984	0.9565	0.1055	0.2384	0.9477	0.6630
8	0.3361	0.9997	0.1630	9.8918e-05	0.6726	0.9952	8.0252e-04	0.0214	0.0159	0.9462
9	0.7401	1.0000	0.9111	0.0053	2.6521e-04	0.0586	0.0782	0.7859	0.2151	0.0802
10	0.7906	0.0228	0.9064	0.0770	0.9936	0.9987	0.0171	0.1251	0.9979	1.5003e-04

Table 3: Indeterminacy membership matrix (I) of the Baboon image

	1	2	3	4	5	6	7	8	9	10
1	0.2435	0.0702	0.1143	0.0139	0.4144	0.0685	0.2258	0.9985	6.8476e-04	0.9908
2	0.2698	0.2512	0.7190	0.0234	0.5199	0.2617	0.0014	0.0015	0.2125	0.7959
3	0.1953	0.0662	0.3941	0.0450	0.9983	0.9378	0.9656	0.0017	0.5065	0.9781
4	0.1177	6.7653e-04	0.1341	0.0399	0.8894	0.8656	0.9998	0.7837	0.3438	0.9939
5	0.0593	0.2963	0.0258	0.0591	0.7475	0.0028	0.5776	0.1510	0.2518	0.6125
6	0.0925	0.1907	0.8527	0.4854	0.4870	9.1281e-04	0.0023	0.7074	0.9038	0.9843
7	0.0527	0.0738	0.3936	0.9183	0.0174	0.2581	0.4860	0.7923	0.2962	0.9219
8	0.9210	0.0041	0.6414	0.0015	0.9122	0.0441	0.0094	0.1491	0.1175	0.3024
9	0.8266	2.0131e-05	0.4328	0.0474	0.0035	0.3219	0.3958	0.7492	0.7510	0.4029
10	0.7403	0.1567	0.4482	0.3914	0.0557	0.0145	0.1248	0.5439	0.0216	0.0021

Table 4: Falsity membership matrix (F) of the Baboon image

	1	2	3	4	5	6	7	8	9	10
1	0	0.9214	0	0.9849	0.5021	0	0	0	0	0
2	0	0.7068	0.0824	0.9743	0	0.6940	0.9985	0.9984	0	0
3	0	0	0.5282	0.9500	0	0	0	0.9982	0.3813	0
4	0.8664	0	0	0.9558	0	0	0	0	0.5920	0
5	0.9338	0	0	0.9340	0	0	0	0	0.7061	0
6	0.8957	0.7800	0	0.4094	0	0	0	0	0	0
7	0.9413	0	0.5288	0	0	0	0.4085	0	0	0
8	0	0	0.1956	0.9984	0	0	0.9898	0.8295	0.8666	0
9	0	0	0	0.9473	0.9962	0.6195	0.5259	0	0.0339	0.5169
10	0	0.8205	0	0.5316	0	0	0.8581	0.3310	0	0.9977

Watermark recovery performance is measured using our standard correlation coefficient (NC) between the original and recovered watermarks. The table below shows the NC values for the images after the attacks

6.2 Noise Attacks

Tables 5 through 7 demonstrate the robustness of the proposed zero-point watermarking system and its resistance to various types of image attacks.

Table 5 shows that the extracted watermark at NC values exhibits high resistance to various types of distortion attacks, with most values exceeding 0.93 and reaching 1.0 for Poisson distortion in many images. This indicates that the extracted features are highly resistant to random variations in light intensity, effectively preserving and protecting the watermark information.

Table 5: NC values after applying a noise attack to the images

Attacks	Baboon	Peppers	Girl	Village Road
Salt and pepper Nois (1%)	0.951	0.943	0.933	0.939
Gaussian Noise	0.977	0.970	0.943	0.931
Poisson noise	1	1	1	0.990
Speckle noise	0.963	0.960	0.969	0.938

6.3 Filter Attacks

Regarding filtering attacks (Table 6), the proposed method remains successful under low-pass Gaussian filtering, medium-pass filtering, and intermediate-pass filtering, where NC values are close to 0.94 or higher. Motion filtering causes a greater deterioration in performance, with NC values ranging from 0.747 to 0.823, because motion blur obscures the structural details used during feature extraction. However, the extracted watermark remains clearly distinguishable.

Table 6: NC values after applying a filter attack to the images

Attacks	Baboon	Peppers	Girl	Village Road
Gaussianlowpassfilte	0.941	0.959	0.949	0.944
Motion filter	0.786	0.823	0.786	0.747
Average filter	0.934	0.953	0.951	0.946
MED filter	0.935	0.954	0.945	0.940

6.4 Image-Processing Attacks

Table 7 shows excellent resistance to common image manipulation techniques. JPEG compression at a quality factor of 100 produces NC values higher than 0.98 for all test images, while the histogram equation produces NC values between 0.971 and 0.989. These results demonstrate that the proposed neutron-based feature extraction approach produces stable and distinctive features capable of maintaining the watermark's integrity against various types of distortion and image manipulation attacks.

Table 7: NC values after applying an image-processing attack to the images

Attacks	Baboon	Peppers	Girl	Village Road
JPEG Compression Quality (100)	0.997	0.995	0.992	0.983
Histogram Equalization	0.989	0.986	0.981	0.971

Overall, the consistently high NC values demonstrate the effectiveness of the proposed scheme in maintaining the accuracy of watermark recovery and image ownership verification under a wide range of common image processing operations.

Table 8: Recovered watermark images for the three cases for the Baboon image

attack	Salt & pepper Noise (0.01)	Gaussian noise	Poisson noise	Speckle noise	Gaussian low-pass filter
Recovered Watermark					
attack	Motion filter	Average filter	MED filter	JPEG Compression	Histogram Equalization
Recovered Watermark					

Table 9: Recovered watermark images for the three cases for the Peppers image

attack	Salt & pepper Noise (0.01)	Gaussian noise	Poisson noise	Speckle noise	Gaussian low-pass filter
Recovered Watermark					
attack	Motion filter	Average filter	MED filter	JPEG Compression	Histogram Equalization
Recovered Watermark					

Table 10: Recovered watermark images for the three cases for the Girl image

attack	Salt & pepper Noise (0.01)	Gaussian noise	Poisson noise	Speckle noise	Gaussian low-pass filter
Recovered Watermark					
attack	Motion filter	Average filter	MED filter	JPEG Compression	Histogram Equalization
Recovered Watermark					

Table 11: Recovered watermark images for the three cases for the Village Road image

attack	Salt & pepper Noise (0.01)	Gaussian noise	Poisson noise	Speckle noise	Gaussian low-pass filter
Recovered Watermark					
attack	Motion filter	Average filter	MED filter	JPEG Compression	Histogram Equalization
Recovered Watermark					

7. Discussion

The results obtained in this research show that the proposed zero watermarking system possesses high robustness against various types of attacks, thanks to the stable properties extracted from the neutral (T) truth component. Noise attacks have little effect because the block-based property extraction process limits the impact of random pixel variations while preserving the underlying image structure. Consequently, NC values are maintained at high levels, especially under Poisson noise.

Regarding filtering attacks, low-pass, medium-pass, and intermediate Gaussian filters preserve most of the structural information, resulting in only a slight performance degradation. In contrast, motion blur causes a greater decrease in NC values because it distorts edges and local image details that underpin property generation. However, the recovered watermark remains strongly associated with the original watermark.

8. Comparison

Recent state-of-the-art zero-watermarking techniques, particularly methods based on DWT [29], DCT [13], SVD [30], PCA [23], or other, such comparisons are necessary to demonstrate the advantages and effectiveness of the proposed framework. To demonstrate the importance and the validation of the results for the proposed paradigm, a comparison with several schemes in the literature is conducted.

The table shows a comparison between the proposed method and several previous methods, where the method based on neutrosophic transformation was distinguished by its ability to maintain high robustness. It also achieved superior normal correlation coefficient (NC) values ranging between 1 and 0.93 under various attacks compared to other methods, such as REF[23] and REF[13].

Table 12: Compared the proposed zero watermarking scheme with previous methods

Method	Technique	Watermark Type	Value NC (Typical under Attacks)	Robustness
Propose Method	Neutrosophic-transformation	Zero-watermark	1-0.93	yes
REF[23]	PCA-Zero Watermarking	Zero-watermark	0.995-0.699	no
REF[29]	DWT-based Zero Watermarking	Zero-watermark	1-0.992	**yes**
REF[30]	DWT-SVD	Embedded	0.997-0.990	**Yes**
REF[13]	DTCWT-QR	Zero-watermark	1-0.990	**Yes**

9. Conclusion and Future Work

This paper presented a neutrosophic-domain-based zero-watermarking framework for secure image copyright protection and authentication. The proposed method utilized the truth component of the neutrosophic image together with block-based statistical feature extraction and chaotic scrambling to generate a secure watermark share without modifying the original image. The experimental and analytical results demonstrated that the proposed framework provides good robustness, security, and computational efficiency against common image processing attacks. Future work may focus on developing adaptive feature extraction strategies and integrating advanced algebraic or intelligent optimization techniques to further improve robustness and security performance. In addition, the proposed framework can be extended to color images, medical images, and multimedia authentication applications.

References

[1] M. Barni, F. Bartolini, and A. Piva, "Improved Wavelet-Based Watermarking Through Pixel-Wise Masking," *IEEE Transactions on Image Processing*, vol. 10, no. 5, pp. 783–791, 2001.

[2] X. Kang, J. Huang, Y. Q. Shi, and Y. Lin, "A DWT-DFT Composite Watermarking Scheme Robust to Both Affine Transform and JPEG Compression," *IEEE Transactions on Circuits and Systems for Video Technology*, vol. 13, no. 8, pp. 776–786, 2003.

[3] C.-C. Chang, P. Tsai, and C.-C. Lin, "SVD-Based Digital Image Watermarking Scheme," *Pattern Recognition Letters*, vol. 26, no. 10, pp. 1577–1586, Elsevier, 2005.

[4] A.M. Abduldaim, N.M.G. Al-Saidi, A.K. Faraj, and S.A. Alameer Kadhim, "Enhancing Image Security through PCA-IWT-Based Nil Steganography under Distortion Scenarios," Boletim da Sociedade Paranaense de Matemática, vol. 43, no. 3, (2025), pp. 1–18.

[5] A.F. Mutlk, A.M. Abdmldaim, and M.E. Abdulmunim, "Employing Algebraic Eigenvalue Decomposition in Zero Watermarking Technology," International Journal of Mathematics and Computer Science, vol. 20, no. 1, (2025), pp. 333–343.

[6] F. Smarandache, *Neutrosophy: Neutrosophic Probability, Set, and Logic: Analytic Synthesis & Synthetic Analysis*. Rehoboth: American Research Press, (1998).

[7] Y. Guo and H.D. Cheng, "New neutrosophic approach to image segmentation," *Pattern Recognition*, vol. 42, no. 5, (2009), pp. 587-595.

[8] H.D. Cheng, Y. Guo, and Y. Zhang, "A novel image segmentation approach based on neutrosophic set and improved fuzzy C-means algorithm," *New Mathematics and Natural Computation*, vol. 7, no. 1, (2011), pp. 155-171.

[9] J. Wen, S. Xuan, Y. Li, Q. Peng, and Q. Gao, "Image segmentation algorithm based on neutrosophic fuzzy clustering with non-local information," *IET Image Processing*, vol. 14, no. 3, (2020), pp. 576-584.

[10] B. Yu, Z. Niu, and L. Wang, "Mean shift-based clustering of neutrosophic domain for unsupervised constructions detection," *Optik*, vol. 124, no. 21, (2013), pp. 4697-4706.

[11] Y. Guo and A. Sengür, "A novel image edge detection algorithm based on neutrosophic set," *Computers & Electrical Engineering*, vol. 40, no. 8, (2014), pp. 3-25.

[12] A.A. Salama, M. Eisa, and A.E. Fawzy, "A neutrosophic image retrieval classifier," *International Journal of Computer Applications*, vol. 170, no. 9, (2017), pp. 1-6.

[13] G. Yang, X. Lu, Y. Lu, J. Tang, and X. Xiong, "Robust zero-watermarking method for multiple medical images using wavelet fusion and DTCWT-QR," *Journal of Information Security and Applications*, vol. 90, (2025), Art. no. 103945.

[14] I.W. Elhamzi, "Enhancing medical image security with FPGA-accelerated LED cryptography and LSB watermarking," *Traitement du Signal*, vol. 41, no. 1, (2024), pp. 85-97.

[15] R. Purnima, A. Rakesh, and N. Gautam, "Motion-frames based video watermarking scheme for copyright protection using guided filtering in wavelet domain," *Traitement du Signal*, vol. 40, no. 1, (2023), pp. 187-197.

[16] R. Riyajuddin and A.P. Reddy, "Various image processing attacks for image watermarking in the wavelet domain using singular value decomposition and discrete cosine transform," *Review of Computer Engineering Studies*, vol. 8, no. 2, (2021), pp. 51-59.

[17] Taha Basheer Taha, Huda E. Khalid, Neutrosophic Similarity Measure for Assessing Digital Watermarked Images, Neutrosophic Sets and Systems, Vol. 61, 2023, 53-68.

[18] Atta R, Ghanbari M. A high payload steganography mechanism based on wavelet packet transformation and neutrosophic set. J Vis Commun Image Represent. 2018;53:42–54.

[19] Ming Zhang, Ling Zhang, H.D. Cheng, A neutrosophic approach to image segmentation based on watershed method, Signal Processing 90 (2010) 1510–1517.

[20] Amanna Ghanbari Talouki, Abbas Koochari, Image completion based on segmentation using neutrosophic sets, Expert Systems with Applications, Volume 238, Part A, 2024.

[21] Z. Pan, C. Wu, C. Yang, and B. Zhao, "Double-matrix decomposition image steganography scheme based on wavelet transform with multi-region coverage," *Entropy*, vol. 24, no. 2, (2022), Art. no. 246.

[22] Q. Su, Y. Sun, Y. Xia, and Z. Wang, "A robust color image watermarking scheme in the fusion domain based on LU factorization," *Optics & Laser Technology*, vol. 174, (2024), Art. no. 110567.

[23] S.A. Kahdim and A.M. Abduldaim, "Principal component analysis for zero watermarking technique," *International Journal of Mathematics and Computer Science*, vol. 18, no. 1, (2023), pp. 85-97.

[24] X. Wang, Q. Du, L. Du, H. Zhang, and J. Hu, "Robust zero-watermarking algorithm via multi-scale feature analysis for medical images," *Journal of Information Security and Applications*, vol. 89, (2025), Art. no. 103937.

[25] M. Yang, J. Li, U.A. Bhatti, C. Shao, and Y. Chen, "Robust watermarking algorithm for medical images based on non-subsampled shearlet transform and Schur decomposition," *Computer Materials & Continua*, vol. 75, no. 3, (2023), pp. 5539-5554.

[26] M. K. Hussein, A. Alqassab, and L. T. Alkahla, "Image Classification Using Deep Learning: A Systematic Review," Neutrosophic Optimization and Intelligent Systems*, vol. 8, (2025).

[27] A. Paraskevas, "Extended Certainty Factors utilizing Neutrosophic Logic," Neutrosophic Optimization and Intelligent Systems, vol. 4, (2024).

[28] A. S. Ravindrabahadur, R. Singh, and S. N. Tiwari, "Logarithmic Ratio-Type Estimator for Finite Population Mean under Neutrosophic Framework," Neutrosophic Optimization and Intelligent Systems, vol. 7, (2025).

[29] M. Al-Haj, "A Zero-Watermarking Scheme using Discrete Wavelet Transform," *Procedia Computer Science*, vol. 65, (2015), pp. 1–8.

[30] A. Alzahrani, "Enhanced Invisibility and Robustness of Digital Image Watermarking Based on DWT-SVD," *Applied Bionics and Biomechanics*, vol. 2022, Art. no. 5271600, 2022.